J Ther Eng, Vol. 7, Supp 14, pp. 1843–1856, December, 2021

Journal of Thermal Engineering
Web page info: https://jten.yildiz.edu.tr
DOI: 10.18186/thermal.1051232

Journal of Thermal Engineering

Research Article

Analysis of heat transfer performance of the absorber tube with convergent-divergent structure for parabolic trough collector

Zhao XUYI[1], Wang FUQIANG[1,*], Shi XUHANG[1], Cheng ZIMING[1], Gong XIANGTAO[2]

[1]School of New Energy, Harbin Institute of Technology at Weihai, 2, West Wenhua Road, Weihai 264209, P. R. China
[2]Department of Mechanical and Aerospace Engineering, Missouri University of Science and Technology, Rolla, MO 65409, USA

ARTICLE INFO

Article history
Received: 31 May 2020
Accepted: 22 November 2020

Key words:
Solar energy; Parabolic trough collector; Monte Carlo ray tracing; Finite Volume method; Convergent-divergent structure; Heat transfer enhancement

ABSTRACT

In order to effectually improve the performance of parabolic trough solar collector system and homogenize the temperature distribution on the absorber tube, an innovative convergent-divergent tube was designed as the absorber tube of PTR. The finite volume method (FVM) and the Monte Carlo ray tracing method (MCRT) are combined to simulate the heat transfer process in parabolic trough collector. The average relative error between the numerical results and the experimental results conducted in the Spanish DISS test facility is 1.103%, which confirms the reliability of the simulation results in this paper. The heat transfer characteristics and flow characteristics of PTR and convergent-divergent PTR are compared in the inlet velocity range of 0.05–0.75m/s, and the effect of the number of zoom sections(N) for CD-PTR performance is also studied. The simulation results show that the parabolic trough collector with convergent-divergent tube has significantly enhanced heat transfer capability. The average Nu of CD-PTR increases as the number of zoom sections increases, and is always higher than that of PTR. When Re=86400 and N=25, the average Nu increased by 66%.

Cite this article as: Xuyi Z, Fuqiang W, Xuhang S, Ziming C, Xiangtao G. Analysis of heat transfer performance of the absorber tube with convergent-divergent structure for parabolic trough collector. J Ther Eng 2021;7(Supp 14):1843–1856.

INTRODUCTION

Eliminating the negative environmental impact of using fossil fuels, meeting the growing energy demand brought about by development, and seeking renewable and environmental friendly alternatives have become topics of great concern in recent years [1,2]. Although renewable energy, especially solar energy, accounts for only a small part of today's energy supply, it has various direct or indirect advantages that make it a key to sustainable development program [3]. The great potential of solar energy to satisfy the energy needs in many fields is increasingly recognized by relevant researchers [4–6].

In the past decade, the application of direct (photovoltaic) and indirect (concentrated solar) solar power

***Corresponding author.**
*E-mail address: wangfuqiang@hitwh.edu.cn

This paper was recommended for publication in revised form by Regional Editor Jaap Hoffman Hoffman

generation has been steadily increasing [7,8]. The use of solar energy for electricity production promises to be one of the most viable options to replace fossil fuel power plants [9–11]. The concentrated solar power (CSP) system that focuses solar radiation energy onto the receiver can reduce the requirement of collector materials and provide lower heat losses due to the reduced target area [12–14]. The parabolic trough collector (PTC), as a CSP technology that has been extremely developed, has already had relatively abundant operational experience, and currently has great prospects [15,16]. Due to the characteristics of wide distribution and low energy flow density of solar energy, centralized solar power plants generally occupy a large area. Parabolic trough mirrors, receivers (PTR) and related power generation equipment are usually the three main components of their facilities [17,18].

Parabolic trough receiver (PTR) is the major part of the traditional PTC. The receiver is a concentric sleeve structure, with its outer layer is a thin transparent glass envelope, and the inner layer is a metal absorber tube [19]. And a vacuum environment is set between the two layers, which can effectively reduce the heat loss of convection. The input solar radiation is reflected and converges at the focal line of the parabolic mirror. The concentrated solar radiation is received by the receiver located here and stored as thermal energy into heat transfer fluid (HFT) [20,21].

The demand for more efficient energy conversion equipment has promoted the development of solar energy utilization technology [22,23]. The method of optimizing the structure to improve the thermal performance of the system is widely used in scientific research and production [24–27]. The research on structure modification of PTR absorber tube is earlier and the technology is more mature [28,29].In order to improve the heat transfer performance and reliability of the PTR system, Wang et al. [30] numerically calculated the thermal performance of the system using symmetrical outward corrugated tube as the metal tube of the PTC. The effect of various detailed parameters of the bellows on the heat transfer performance of the system is studied, including corrugation height (H), corrugation spacing (p), corrugation wave crest radius (R) and corrugation groove radius (r). The results show that when Re = 81728 and p/D=4.3, the effective heat transfer coefficient using symmetrical outward corrugated tube can increase by 8.4%. Zhang et al. [31] conducted experiments on natural convection boiling heat transfer in smooth tube, ordinary convergent-divergent tube and improved convergent-divergent tube. The improved convergence-divergence tube has better heat transfer performance than ordinary convergence-divergence tube, and its enhancement ratio is about 1.18 times. Jin et al. [32] simulated the heat transfer and flow resistance performance in particular convergent-divergent tube with different structural parameters. It is pointed out that fluid separation near the solid wall effectively strengthens heat transfer, changes in fluid flow line enhance fluid mixing, and the drop of fluid resistance increases significantly. Pandey et al. [33] numerically calculated the effect of inserting an arc plug into the PTR absorption tube on the heat transfer performance of the system. In order to obtain the optimal size R of the arc plug, a series of calculations are carried out. It is observed that for arc plugs with factors R=1 and R=0.879, PTC has the highest thermal efficiency.

Another approach to improve the thermal performance is related to improving the thermophysical properties of the materials [34–37]. Due to good properties of radiation absorption and high thermal conductivity, nanofluid are often used as the working medium in the heat exchange equipment [38]. Hussein et al. [39–41] gave comprehensive overviews of theories, simulations and experiments related to the application of nanotechnology in different types of solar collectors. The reviews pointed out the importance of accurate selection of nanoparticle volume fraction and diameter for the performance of the collector, and further guided that future research must be devoted to inventing efficient energy transport methods of nanofluid in solar collectors.

The temperature distributed around the circumference of the absorber tube is inhomogeneous. This is because the upper half of absorber tube directly receives incident solar radiation, while the lower half receives the light that is concentrated by the reflector, resulting in not-uniform distribution of circumferential flux [42]. The not-uniform temperature distribution will cause deformation and bending of the absorber tube, which may further damage the PTR. The optical performance analysis on PTC by Jebasingh et al. [43] showed that the optical efficiency should be optimized to withstand against environmental conditions, many optical factors have been studied to improve the heating conditions of the absorber tube [44]. To reduce the temperature gradient of the absorber tube, scholars also have conducted many studies on certain specific heat transfer processes in PTR technology [45–47]. A new type of perforated plate inserts was proposed for use in parabolic trough collector, and the thermodynamic performance of the system was simulated [48]. The geometric parameters of different perforated plates are analyzed. Studies have shown that the thermal conditions of the receiver have improved significantly. Wang et al. [49] applied the elliptical-circular section glass cover in the solar energy absorber system. The influence of the refractivity and cross-sectional parameters of the glass cover on the heat flux distribution is also studied by Monte Carlo Ray Tracing (MCRT) method. The numerical simulation results show that using glass cover with an elliptical-circular cross-section with a high refractivity for the receiver can minimize the heat flux distribution gradient and effectively reduce thermal stress. The work of Manikandan et al. [50] includes numerous techniques for enhancing the optical and thermal efficiency of parabolic trough collectors. A series of factors that affect the optical efficiency of the parabolic trough collector are

summarized, including coating of selective surface on receiver tube, reflectivity of the mirror, intercept coefficient of the absorber tube, Incorporating secondary reflector, etc. In addition, they recommended the black body cavity receiver to reduce heat loss and improve optical and thermal efficiency.

To enhance the collection and utilization performance of PTR technology for solar energy and improve the availability of the system, the authors proposed to apply convergence-divergence structure to PTR technology to obtain a novel parabolic trough receiver (CD-PTR). The Monte Carlo ray tracing (MCRT) method is used to determine heat flux distribution on collector tubes in the study [51]. The numerical simulation is carried out using the concept of Finite Volume Method (FVM) to investigate the advantages of CD-PTR compared to ordinary PTR system [52] [53]. The influence of the geometric parameters variation on the system performance was also studied, which also provides theoretical instructions for further research and practical application.

PHYSICAL MODEL

The simplified schematic diagram of general PTC system [51] is presented in Figure 1. As we can see, solar radiation is incident along the *y* axis in the negative direction, and then it is reflected by the trough condensing system and collected on the receiver. Highly concentrated solar radiation accumulates at the bottom periphery of the receiver, while other part is directly irradiated by sunlight with low heat flux density.

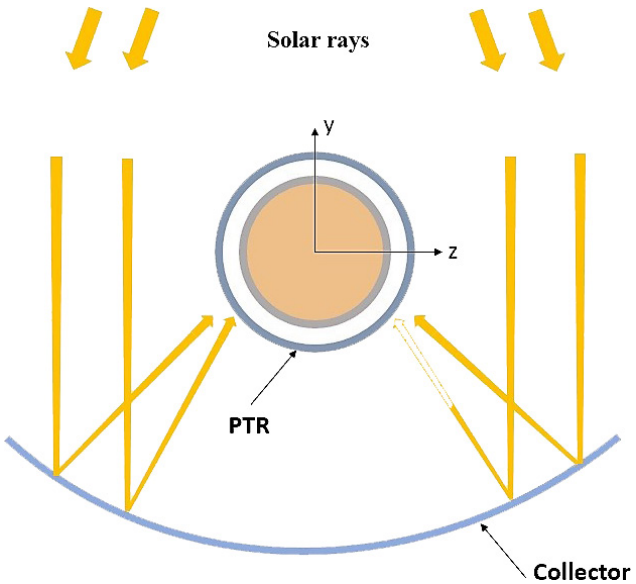

Figure 1. Schematic diagram of parabolic trough solar collector (PTC) system [51].

The parabolic trough receiver (PTR) is an important component of the PTC system, and Figure 2 is the schematic cross-sectional view of PTR and describes the complete heat transfer process within the system [51]. The solar collector is concentric sleeve structure, which the outer layer is a thin transparent glass envelope, and the inner layer is a metal absorber tube. A vacuum environment is provided between the sleeves, and the heat transfer fluid flows into internal metal absorber tube from the inlet. The absorber tube is coated with selective coating for higher solar spectral absorption. And the selective coating on glass envelope can increase the solar radiation transmitted into the PTR system, thus reducing the heat loss outside the receiver. The vacuum environment was set to reduce heat loss caused by convection during heat transfer process.

Table 1 lists some detailed parameters of the RTC system. They are obtained by the existing PTR system, which are the same as the reference [54].

Some researchers have studied various tubes as PTR absorber tubes to obtain higher solar energy utilization

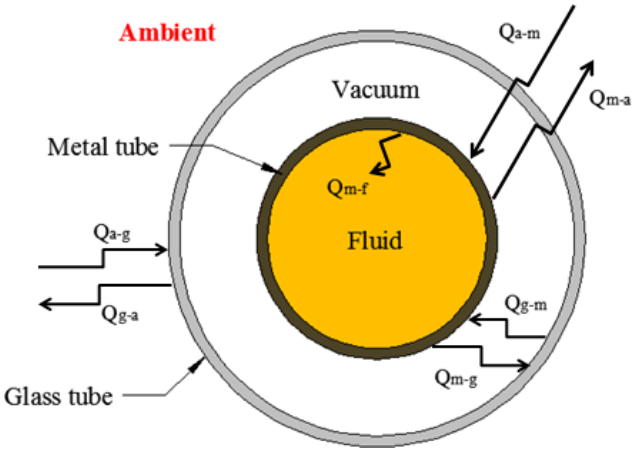

Figure 2. Schematic diagram of the heat transfer process of PTR [51].

Table 1. Detailed parameters of the PTC studied by the authors [54]

Geometric and optical parameters	Values
Length of PTR	4.06m
Outer diameter of glass envelope	0.14m
Outer diameter of metal tube	0.07m
Thickness of metal tube	0.003m
Aperture of PTC	0.525m
Rim angle	15°
Non-parallelism angle	16′
Reflectivity of PTC	0.90
Absorptivity of metal tube	0.95

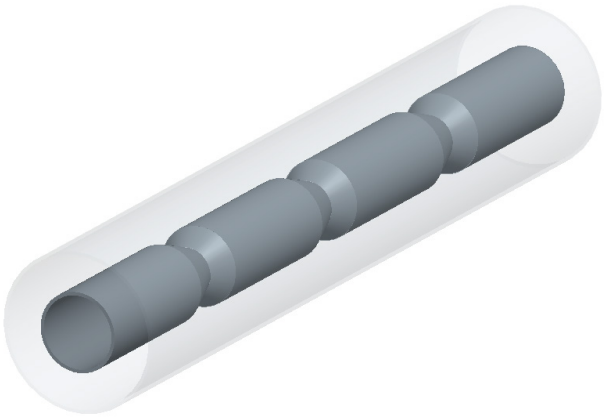

(a)

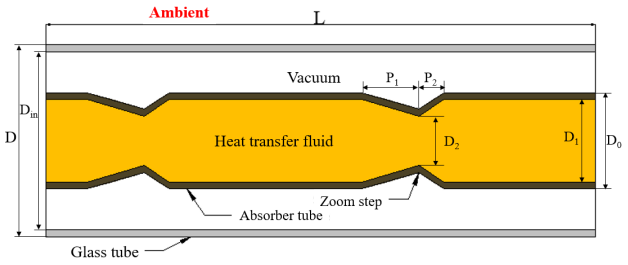

(b)

Figure 3. 3D view and axial section schematic of CD-PTR studied in this paper.

efficiency and convergent-divergent structure have been applied in various engineering practices. But no researchers had proposed to apply convergent-divergent tube as the PTR absorber tube in solar thermal power utilizations. In this study, an innovative convergent-divergent tube is proposed to enhance the heat transfer and homogenize the temperature distribution in PTR system. The structural schematic of convergent-divergent tube used for simulation in this study is presented in Figure 3, and the relevant dimensions are added to the diagram. The convergent-divergent tube simulated in this study is the structure of contraction-expansion.

MATHEMATICAL MODEL

In computational fluid dynamics (CFD) analysis in this paper, governing equations that reflect the dynamic characteristics of PTR solar thermal utilization process include continuity equation, momentum and energy conservation equation and radiation transfer equation. The Finite Volume Method(FVM) is used to discretize the computational domain and governing equations.

Continuity Equation

$$\frac{v_r}{r}+\frac{\partial v_r}{\partial r}+\frac{1}{r}\frac{\partial v_\varphi}{\partial \varphi}+\frac{\partial v_x}{\partial x}=0 \tag{1}$$

Momentum Conservation Equation

$$\rho\left(\frac{\partial v_r}{\partial t}+v_r\frac{\partial v_r}{\partial r}+\frac{v_\varphi}{r}\frac{\partial v_r}{\partial \varphi}-\frac{v_\varphi^{\,2}}{r}+v_x\frac{\partial v_r}{\partial x}\right)=\rho g_r$$
$$+\mu\left(\frac{\partial^2 v_r}{\partial r^2}+\frac{1}{r}\frac{\partial v_r}{\partial r}+\frac{1}{r^2}\frac{\partial^2 v_r}{\partial \varphi^2}+\frac{\partial^2 v_r}{\partial x^2}-\frac{2}{r^2}\frac{\partial v_\varphi}{\partial \varphi}-\frac{v_r}{r^2}\right)-\frac{\partial P}{\partial r} \tag{2}$$

$$\rho\left(\frac{\partial v_\varphi}{\partial t}+v_r\frac{\partial v_\varphi}{\partial r}+\frac{v_\varphi}{r}\frac{\partial v_\varphi}{\partial \varphi}+v_x\frac{\partial v_\varphi}{\partial x}+\frac{v_r v_\varphi}{r}\right)=\rho g_\varphi$$
$$+\mu\left(\frac{\partial^2 v_\varphi}{\partial r^2}+\frac{1}{r}\frac{\partial v_\varphi}{\partial r}+\frac{1}{r^2}\frac{\partial^2 v_\varphi}{\partial \varphi^2}+\frac{\partial^2 v_\varphi}{\partial x_2}+\frac{2}{r^2}\frac{\partial v_r}{\partial \varphi}-\frac{v_\varphi}{r^2}\right)-\frac{1}{r}\frac{\partial P}{\partial \varphi} \tag{3}$$

$$\rho\left(\frac{\partial v_x}{\partial t}+v_r\frac{\partial v_x}{\partial r}+\frac{v_\varphi}{r}\frac{\partial v_x}{\partial \varphi}+v_x\frac{\partial v_x}{\partial x}\right)=$$
$$\rho g_x+\mu\left(\frac{\partial^2 v_x}{\partial r^2}+\frac{1}{r}\frac{\partial v_x}{\partial r}+\frac{1}{r^2}\frac{\partial^2 v_x}{\partial \varphi^2}+\frac{\partial^2 v_x}{\partial x^2}\right)-\frac{\partial P}{\partial x} \tag{4}$$

Where v is the fluid velocity, ρ is the fluid density, x represents the length direction of the tube, r and φ represent the radial and circumferential directions of tube cross section, respectively.

By comparing the numerical results with the experimental test conducted by Roldán et al. [55] in DISS, Wang et al. [30] proved that the standard k-ε model can not only agree well with the experimental test, but also reduce the average deviation between the simulation results and the experimental test temperature. Therefore, the standard k-ε model was chosen for numerical analyses. Taking turbulent kinetic energy (k) and its dissipation rate (ε) as important parameters, the standard k-ε model is a classic turbulence model in practical engineering calculations. The above two parameters are obtained by following two separate transport equations [56]:

$$\frac{\partial(\rho k)}{\partial t}+\frac{\partial(\rho k)}{\partial t}=$$
$$\frac{\partial}{\partial x_j}\left[\left(\mu+\frac{\mu_i}{\sigma_k}\right)\frac{\partial k}{\partial x_j}\right]+G_k+G_b-\rho\varepsilon-Y_M+S_k \tag{5}$$

$$\frac{\partial(\rho\varepsilon)}{\partial t}+\frac{\partial(\rho\varepsilon\mu_i)}{\partial x_j}=\frac{\partial}{\partial x_j}\left[\left(\mu+\frac{\mu_i}{\sigma_\varepsilon}\right)\frac{\partial \varepsilon}{\partial x_j}\right]$$
$$+C_{1\varepsilon}\frac{\varepsilon}{k}\left(G_k+G_{3\varepsilon}G_b\right)-C_{2\varepsilon}\rho\frac{\varepsilon^2}{k}-S_\varepsilon \tag{6}$$

The calculation method of the turbulent kinetic energy (TKE) generated by the fluid average velocity gradient is analyzed with reference to the Modeling Turbulence Generation of k-ε model. This part of TKE is represented by the symbol G_k [56]. With reference to the effect of Buoyancy

on turbulence in k-ε model, the TKE generated by buoyancy is analyzed and represented by the symbol G_b. Y_M characterizes the effect of fluctuating dilatation on overall dissipation rate in compressible turbulence, and it was analyzed by referring to the effect of compressibility on turbulence in k-ε model. $C_{1\varepsilon}$, $C_{2\varepsilon}$, and $C_{3\varepsilon}$ are definite constants determined by physical model and flow characteristics. σ_k is defined as turbulent Prandtl numbers of k, and σ_s is defined in the same way. S_k and S_ε are source terms.

Energy Conservation Equation

The solid and fluid phases follow different governing equations.

For the solid phase

$$\frac{\partial T_s}{\partial t}=\frac{k}{\rho c_p}\left(\frac{\partial^2 T_s}{\partial r^2}+\frac{1}{r}\frac{\partial T_s}{\partial r}+\frac{1}{r^2}\frac{\partial^2 T_s}{\partial \varphi^2}+\frac{\partial^2 T_s}{\partial x^2}\right) \tag{7}$$

For the fluid phase

$$\begin{aligned}\rho c_p\left(\frac{\partial T_f}{\partial t}+v_r\frac{\partial T_f}{\partial r}+\frac{v_\varphi}{r}\frac{\partial T_f}{\partial \varphi}+v_x\frac{\partial T_f}{\partial x}\right)=\\ k\left(\frac{\partial^2 T_f}{\partial r^2}+\frac{1}{r}\frac{\partial T_f}{\partial r}+\frac{1}{r^2}\frac{\partial^2 T_f}{\partial \varphi^2}+\frac{\partial^2 T_f}{\partial x^2}\right)\\ +\alpha_v T\left(\frac{\partial P}{\partial t}+v_r\frac{\partial P}{\partial r}+\frac{v_\varphi}{r}\frac{\partial P}{\partial \varphi}+v_x\frac{\partial P}{\partial x}\right)+\Phi\end{aligned} \tag{8}$$

where Φ is the dissipation function, and α_v is the expansion coefficient which is defined as $\alpha_v=-\frac{1}{\rho}\left(\frac{\partial \rho}{\partial T}\right)_P$. T is the fluid temperature, P is the absolute pressure, c_p and k represent the heat capacity and thermal conductivity of the heat transfer fluid, respectively.

This paper studies incompressible fluids and dissipation effect is ignored, which allows us to simplify the above equation as:

$$\begin{aligned}\rho c_p\left(\frac{\partial T_f}{\partial t}+v_r\frac{\partial T_f}{\partial r}+\frac{v_\varphi}{r}\frac{\partial T_f}{\partial \varphi}+v_x\frac{\partial T_f}{\partial x}\right)=\\ k\left(\frac{\partial^2 T_f}{\partial r^2}+\frac{1}{r}\frac{\partial T_f}{\partial r}+\frac{1}{r^2}\frac{\partial^2 T_f}{\partial \varphi^2}+\frac{\partial^2 T_f}{\partial x^2}\right)\end{aligned} \tag{9}$$

BOUNDARY CONDITIONS FOR ANALYSIS

The boundary conditions of the numerical calculation are listed in Table 2 [57]. As described in Table 2, the numerical calculation in this paper defines the tube inlet as velocity inlet, the outlet side as fully developed conditions, and the inner wall of metal tube is set to be non-slip boundary.

The upper half of the circumference of the metal tube is directly irradiated with uniform solar irradiation. The average incident solar irradiance is 1000 W/m^2, and is projected through the glass envelope with the transmissivity of 0.96. The absorption rate of absorber tube coated with selective coating is 0.95. The lower half of the circumference of the metal tube is irradiated by concentrated solar radiation reflected from collector:

Table 2. Boundary conditions of analysis [57]

Zone	Boundary conditions
$L = 0, 0 \le R \le R_i$	$V_x = V_{in}$, $V_r = V_\varphi = 0 m/s$, $T_f = T_{in} = 400K$
$L = 4.06, 0 \le R \le R_i$	Fully developed conditions
$R = R_i, 0 \le L \le 4.06$	$V_x = V_r = V_\varphi = 0\ m/s$
$R = R_o, 0 \le L \le 4.06$	$0° \le \varphi \le 180°$, $q_u = 1000 \times 0.96 \times 0.95 = 912 W/m^2$ $180° \le \varphi \le 360°$, $q_l = q_{cal}$

In this paper, the Finite Volume Method(FVM) is used to discretize the governing equations, and the steady-state implicit scheme is used to solve them. The SIMPLE scheme is used to solve the pressure-velocity coupling equation, the discrete format of the convection term is QUICK, and the momentum equation adopts the second-order upwind style. The convergence criterion of the residual of the energy equation is set to be 1×10^{-8}, and the criterion of other equations are set to be 1×10^{-6}.

Model of Concentrated Ray

Solar radiation is distributed outside the receiver to provide thermal energy to heat transfer fluid(HTF). And the heat flux field is extremely inhomogeneous, where the top is exposed to direct sunlight and the bottom is exposed to sunlight focused by optical elements. The distribution of heat flux collected by optical elements was predicted by MCRT method.

When the MCRT method is applied to calculate the radiation field, the radiation input of the system is realized by the ray input, which is set to carry the same energy. The change in the direction of the ray projection is determined by the optical characteristics of the elements and appropriate probability density functions [49]. The method of combining the fitting curve and the user-defined functions introduces the obtained concentrated heat flux distribution to CFD models to further analyze heat transfer and flow performance, which causes tiny interpolating error.

Thermophysical Properties of D12

In this paper, the D12 thermal oil is applied as PTR heat transfer fluid(HTF), whose physical properties are sensitive to temperature changes within its operating temperature range. To obtain accurate simulation results, the thermophysical properties of D12 are fitted to make its physical parameters become polynomial functions of temperature [29,51] and imported into CFD analysis through UDF method. The thermophysical properties of the HTF used in the numerical calculations in this paper are shown in Table 3.

Table 3. Thermophysical properties of D12 thermal oil [29],[51]

Properties	Values
ρ(kg/m^3)	$-6.96982 \times 10^{-1} \times T - 1.31384 \times 10^{-4} \times T^2 - 2.09079 \times 10^{-6} \times T^3 + 776.257$
Cp(kJ/kg·K)	$3.86884 \times 10^{-3} \times T + 2.05029 \times 10^{-6} \times T^2 - 1.12621 \times 10^{-8} \times T^3 + 3.8628 \times 10^{-11} \times T^4 + 2.01422$
λ(W/m·K)	$-1.4781 \times 10^{-4} \times T - 1.6142 \times 10^{-7} \times T^2 + 1.1299 \times 10^{-1}$
v(m^2/S)	$exp[530.944/(146.4 + T) - 2.68168)] \times 10^{-6}$

MESHING AND VERIFICATION OF GRID INDEPENDENCE

Meshing

During the grid generation process, a structured O-grid was generated for PTR and CD-PTR, the meshes of zoom area of convergent-divergent tube were generated by using the method of separate block association and were refined. Figure 4 and Figure 5 are schematic diagrams of the cross section and axial section (partial) of the mesh.

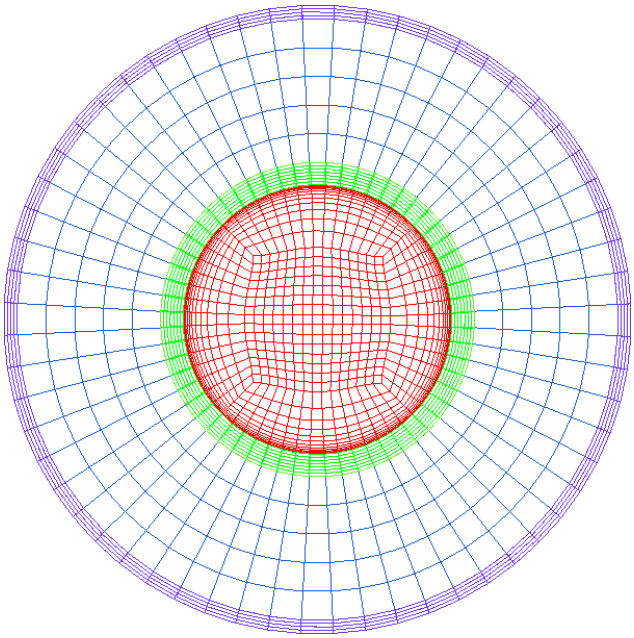

Figure 4. Diagram of cross section of PTR mesh.

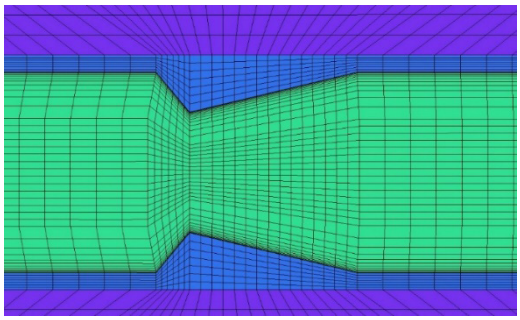

Figure 5. Axial section diagram of CD-PTR mesh.

Verification of Grid Independence

The average heat flux of the absorber tube inner surface is adopted as an evaluation parameter to verify the grid independence due to its importance in characterizing the heat transfer conditions of the coupled-wall. Furthermore, it is suitable to use *Nu* as another evaluation parameter for grid independence verification because the average *Nu* at the tube outlet is a key parameter that investigates heat transfer performance. Considering the denser grid in the zoom area of convergent-divergent tube, in addition to the grid independence verification of the smooth tube, this study also verified the grid independence of convergent-divergent tubes.

For the smooth tube, seven cases with different numbers of grids were set for the grid independent verification tests, respectively: 580,000, 760,000, 950,000, 114,000, 155,000, 183,000, 202,000.

For the convergent-divergent tube, seven cases with different numbers of grids were set for grid independent verification tests, respectively: 850,000, 1,020,000, 1,260,000, 1,550,000, 1,830,000, 2,020,000, 2,210,000.

Figure 6 presents the coupled-wall heat flux and *Nu* variation as the number of grids changes in PTR and CD-PTR, which are marked as symbols $q_{w\text{-}f}$ and *Nu*. It can be seen that when the grid numbers of the smooth tube and the convergent-divergent tube reach 950,000 and 1,830,000, respectively, the values of evaluation parameters remain almost constant. Considering comprehensively computational time and accuracy, the PTR model with 950,000 grids and the CD-PTR model with 1,830,000 grids were selected for further CFD simulation.

MODEL VALIDATION

An experimental study on temperature distribution of PTR absorber tube with superheated steam as HTF has been carried out by Roldán et al. [55]. In order to verify the model used in the numerical calculations in this study, Table 4 lists the detailed test information of several groups of PTR in the Spanish DISS used for model validation. The maximum and minimum temperature on the PTR outlet outer surface were taken as research indicators using the initial conditions of the experiments for numerical simulation.

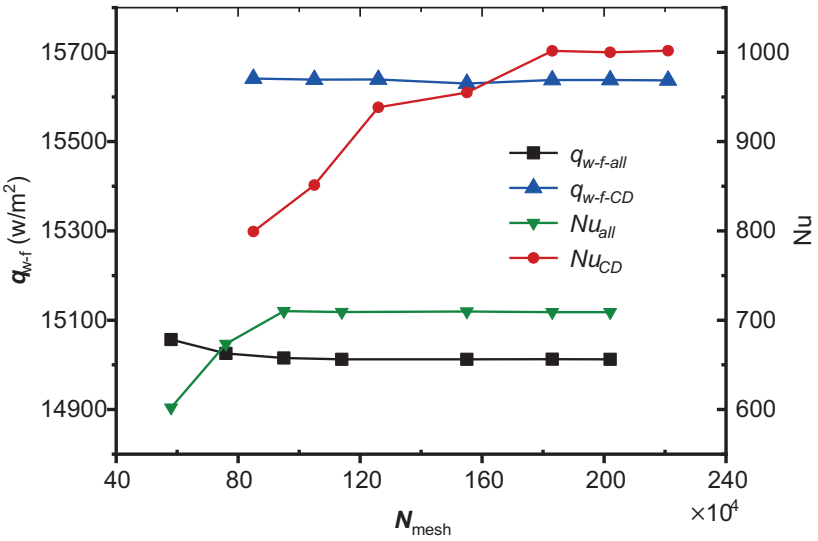

Figure 6. The heat flux (q_w) and *Nu* variation with the increase of number of grids.

Table 4. Specific experimental conditions for PTC thermal performance test conducted by Roldán et al. [55]

case	P_{in} (MPa)	T_{in}(K)	E_{sum}(W/m^2)	*CR*	M(kg/s)
1	6.0	566.3	766	45	0.51
2	6.0	573.0	627	45	0.56
3	6.1	613.0	627	45	0.56
4	6.0	607.3	635	45	0.55
5	6.1	598.1	761	45	0.62
6	6.0	643.0	627	45	0.56
7	6.0	632.9	635	45	0.55

Figure 7 depicts the comparison between the experimental [55] and the CFD simulation results when the maximum and minimum temperature at the outlet are respectively used as parameters. It can be clearly seen that the maximum and minimum temperatures of the PTR outlet simulated by the author are almost consistent with the experimental results.

Table 5 lists the specific experimental results in Spanish DISS [55] and the simulation results obtained in this study under the above initial conditions. Numerical simulation always cannot accurately describe the real flow. For example, although the turbulence model has been verified with experimental results, there are still calculation errors [30]. Furthermore, the experimental temperature of Roldán et al. was measured by thermocouples, the experimental results may also contain measurement errors. These factors have accumulated errors between the simulation results and the experimental results. Table 5 also listed the relative errors between numerical calculations and experimental results,

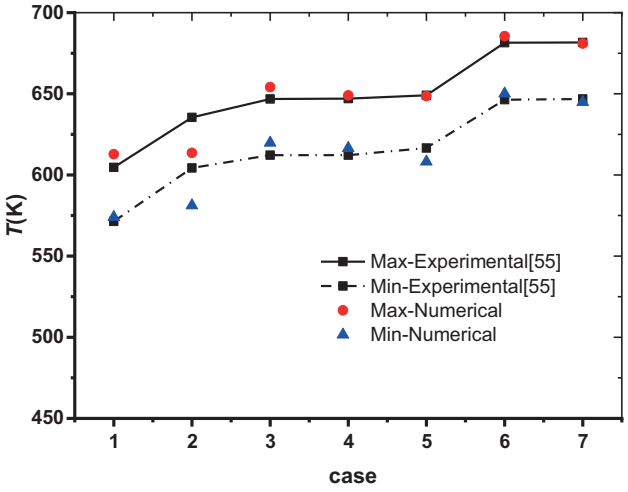

Figure 7. Comparison of temperature between experimental [55] and numerical results.

where the relative error is defined as .The maximum relative error in the cases is 3.823%, and the average relative error is just 1.103%, which proves the reliability of the numerical calculation model in this study.

RESULTS AND DISCUSSION

Analysis of PTR Heat Transfer Performance

To achieve the goal of improving system thermal conditions and enhancing the heat transfer performance, it is necessary to first study heat flux distribution outside PTR metal absorber tube.

Figure 8 represents the distribution of heat flux outside PTR absorber tube for *Re*= 65000. Obviously, the heat flux

Table 5. Comparison between the experimental results of Roldán et al. and the results simulated in this paper

Case	1	2	3	4	5	6	7
$T_{Max.Exp}$ (K)	604.7	635.5	646.8	647	649.1	681.5	681.6
$T_{Max.Num}$ (K)	612.8	613.6	654.1	649	648.6	685.5	681
	1.34%	3.446%	1.129%	0.309%	0.077%	0.597%	0.088%
$T_{Min.Exp}$ (K)	571.4	604.3	612.2	612.2	616.6	646.4	646.8
$T_{Min.Num}$ (K)	574	581.2	619.8	616.5	608.2	650.1	644.9
	0.455%	3.823%	1.241%	0.702%	1.362%	0.572%	0.294%

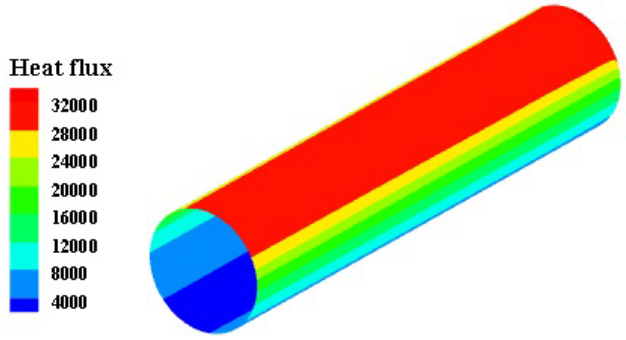

Figure 8. Heat flux distribution outside PTR absorber tube for *Re* = 65000.

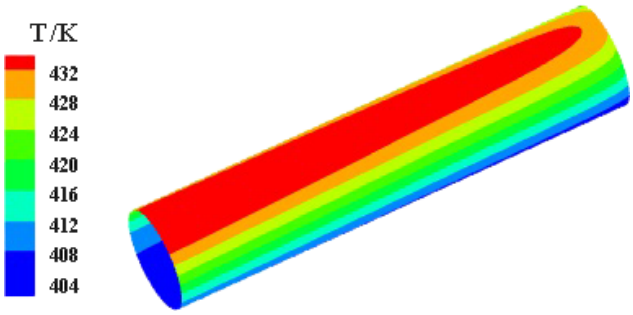

Figure 9. Temperature distribution outside PTR absorber tube for *Re*=65000.

shows a highly uneven distribution. Specifically, the bottom of absorber tube is distributed with highly concentrated solar heat flux, the maximum value of which is close to 40,000 W, while the other parts only exposed to non-concentrated rays with an average heat flux is only about 100W. According to the operating experience of solar thermal power stations, the high non-uniformity of the heat flux may seriously compromise the operation safety of the PTR.

Figure 9 displays the distribution of temperature outside PTR absorber tube for *Re*=65000. Determined by the distribution characteristics of heat flux, the part of absorber tube that receives concentrated solar radiation has a much higher temperature than other parts. Heat transfer fluid (HTF) is continuously heated as it flows, causing the temperature of the fluid to continue to rise, and finally reach the maximum value at the outlet.

Figure 10 presents the temperature distribution at PTR outlet section in the cases with Reynolds numbers of 18900 and 65000 respectively. By comparing the two figures, we can see that as Reynolds number increases, the temperature distribution becomes more uniform. This shows that increasing the Reynolds number leads to increased flow mixing, which effectively reduces the temperature difference and provides better thermal conditions for absorber tube.

Figure 11 presents the change trend of maximum temperature difference of PTR absorber tube as *Re* increases. The maximum temperature difference decreases gradually as *Re* increases, which also means better thermal

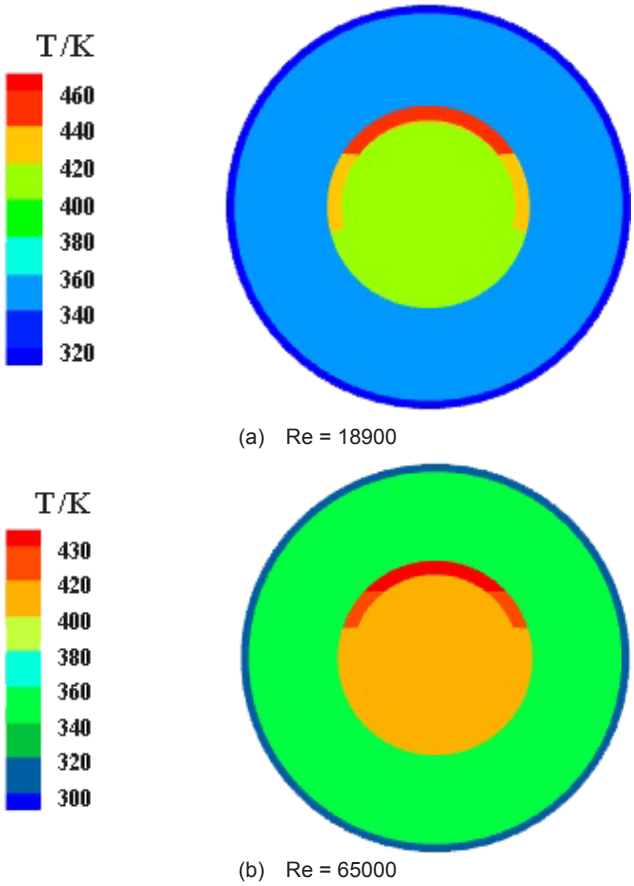

Figure 10. Temperature distribution of PTR outlet with different *Re*.

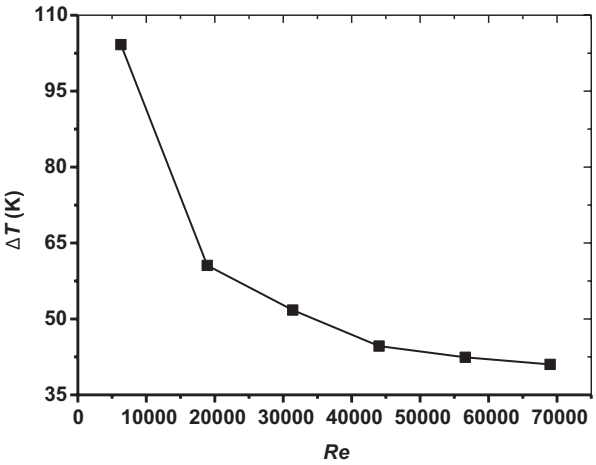

Figure 11. The trend of maximum temperature difference of PTR with the increase of *Re*.

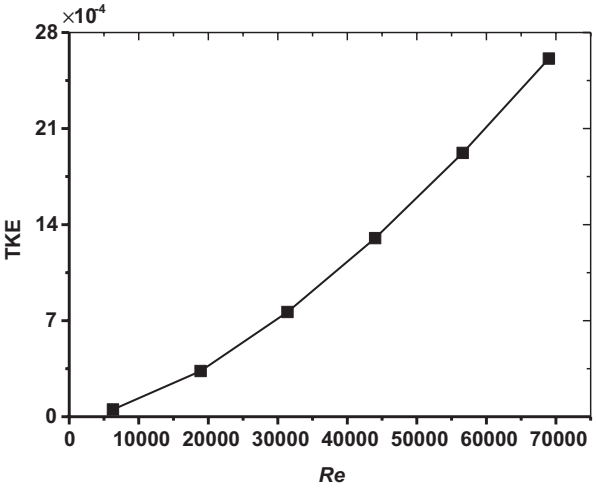

Figure 12. The trend of TKE of PTR with the increase of *Re*.

conditions. And the decreasing in maximum temperature difference slows down gradually.

Turbulent Kinetic Energy (TKE) is an important indicator to measure the development or decline of turbulence. In general, TKE can simultaneously reflect the changes in fluid heat transfer performance and resistance performance. The variation of mass-weighted average TKE of heat transfer fluid in PTR absorber tube with the increase of Reynolds numbers is demonstrated in Figure 12. It can be seen that the TKE of heat transfer fluid increases with the increase of *Re*. And as *Re* increases, the relationship between the TKE and the Reynolds number is close to a linear relationship.

Analysis of CD-PTR Heat Transfer Performance

For higher system heat transfer efficiency, a tube adopted convergent-divergent structure is introduced for

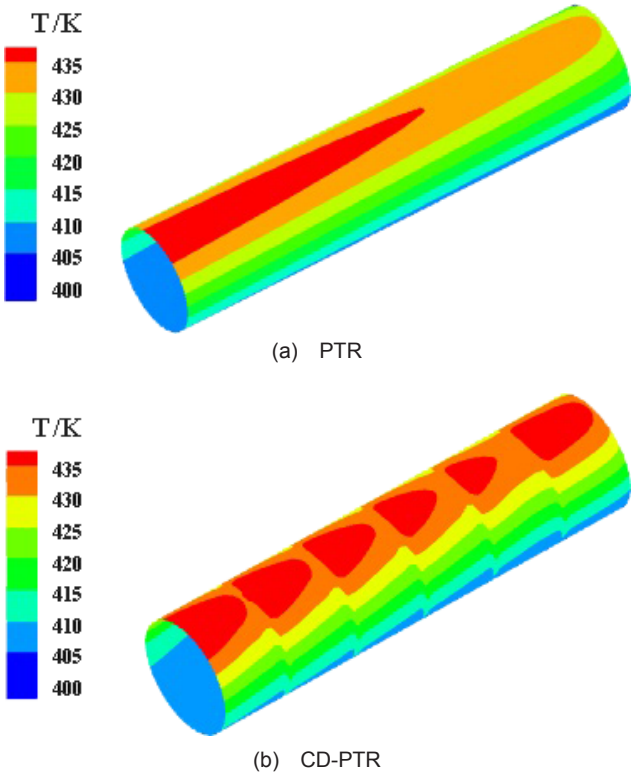

Figure 13. Temperature distribution on the inner wall of absorber tube.

PTR absorber tube. Figure 3 has previously illustrated the schematic diagram of the convergent-divergent PTR (CD-PTR) described in this paper. The temperature distribution on the inner surface of the absorber tube of both PTR and CD-PTR(*N*=5) with *Re*=65000 are presented in Figure 13. It can be found that the average temperature is significantly reduced when convergent-divergent structure is used for PTR absorber tube, and the temperature around the zoom segment is lower than that of the straight segment for CD-PTR.

Figure 14 presents the turbulent kinetic energy (TKE) field of PTR and CD-PTR axial section for *Re* = 65000. As we can see, flow mixing is enhanced, and the turbulent intensity of the boundary layer is significantly increased because of the variable cross section channels in the convergent-divergent tube, thus accelerating heat transfer from tube surface to HTF.

Effects of *N* on CD-PTR Heat Transfer Performance

The number of zoom sections (*N*) of CD-PTR absorber tube has an effect on heat transfer process coupled with flow resistance characteristics, this part is a specific study. Five groups of different models of convergent-divergent tube are investigated: *N*=0, *N*=5, *N*=10, *N*=20, *N*=25. The case *N*=0 indicates the PTR model.

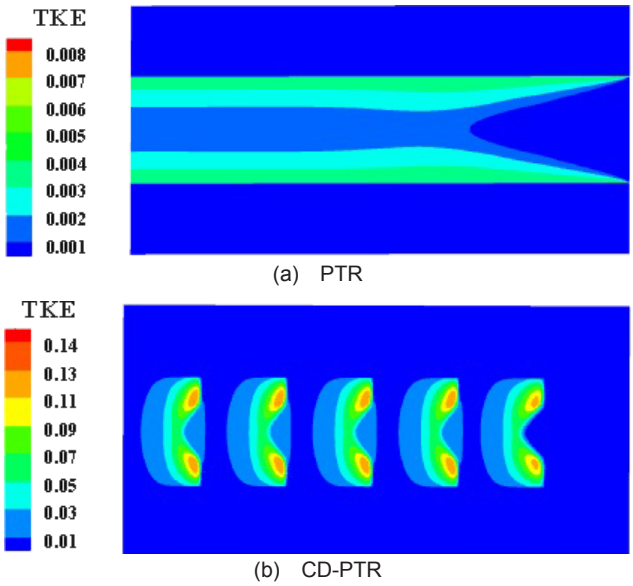

Figure 14. TKE distribution of axial section of PTR and CD-PTR.

In order to study the heat transfer performance in the collector tube, the average Nusselt number of the fluid is used as a parameter for description and analysis.

$$Nu = \frac{h \cdot d_e}{\lambda} \tag{10}$$

Where h represents the convective heat transfer coefficient of the coupled wall which is defined as $h = \frac{q_{w-f}}{T_{t-a} - T_{f-a}}$.

Figure 15 presents the effect of increased *Re* on *Nu* in models with different number of zoom sections (*N*). It can be seen that when the value of *N* is determined, *Nu* gradually increases with the increase of *Re*. This is because the increase of *Re* means the increase of the fluid velocity of the HTF in the heat collecting tube for a certain model. The higher the velocity, the thinner the thermal boundary layer thickness of the fluid was, which further reduced the smaller the wall thermal resistance and intensified the convection heat transfer. In addition, the increase of the number of zoom sections leads to intensified disturbance to the flow, and *Nu,* which characterizes the thermal performance, increases. When *Re*=86400 and *N*=25, the average *Nu* increased by 66%.

Figure 16 presents the trend of the heat flux of coupled wall as *Re* increases, and it is obvious that heat flux increases continuously because of the eddy current in the zoom sections, which strengthens the heat transfer intensity. And as the value of *N* increases, the average heat flux on coupled wall increases gradually, meaning that the heat transfer is enhanced.

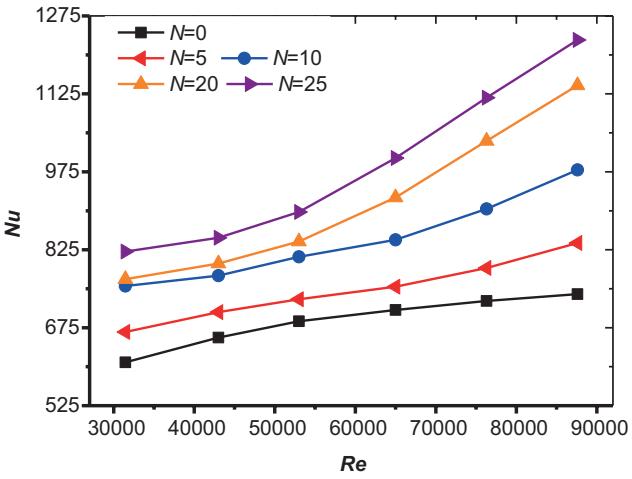

Figure 15. The trend of *Nu* of CD-PTR with different number of zoom sections(*N*).

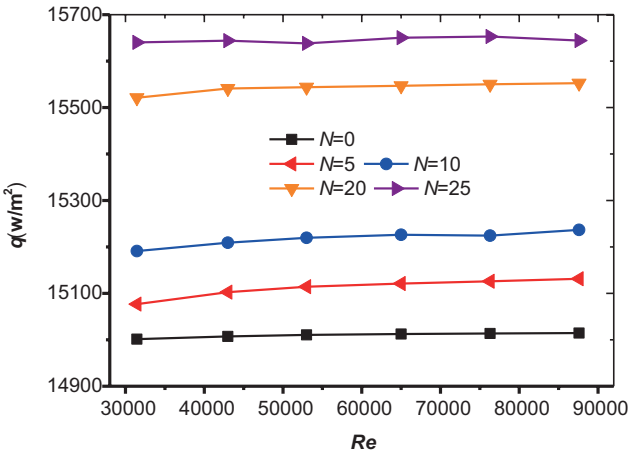

Figure 16. The trend of heat flux(q) of CD-PTR with different number of zoom sections(*N*).

Figure 17 exhibits the effect of increased Reynolds number on pressure drop () of the HTF between tube inlet and outlet of the models for both the PTR and CD-PTR with different numbers of zoom sections (*N*). Obviously, the ΔP between the inlet and outlet of CD-PTR absorber tube is always higher than that of PTR absorber tube. The change in the cross section of the flow channel caused by the convergent-divergent structure will affect the velocity and greatly reduce the fluid pressure in the CD-PTR absorber tube. The introduction of convergent-divergent structure inevitably brings an increase in pressure drop, which will lead to a significant increase in operating power consumption, thereby affecting the improvement of system efficiency.

The evaluation of heat exchanger efficiency should not only focus on its heat transfer performance, but also consider its resistance performance which are characterized by Fanning friction factor(f).

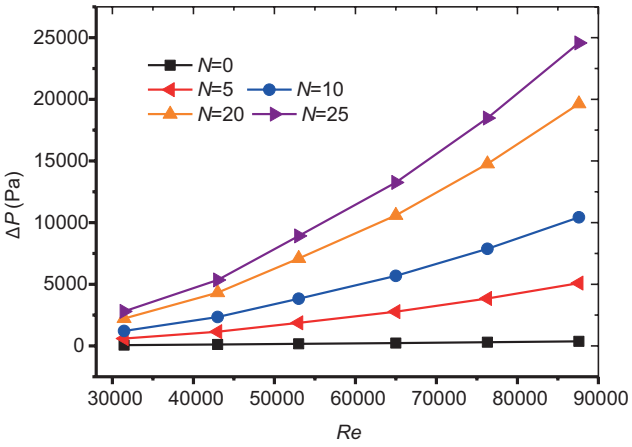

Figure 17. The trend of pressure drop (ΔP) of CD-PTR with different number of zoom sections(N).

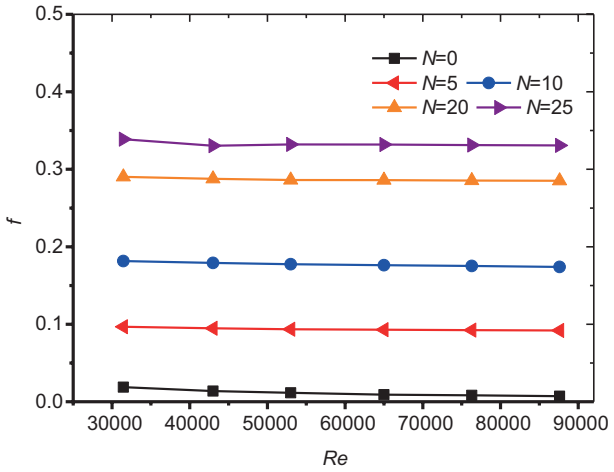

Figure 18. The trend of friction factor (f) of CD-PTR with different number of zoom sections(N).

Figure 18 shows the trend of friction factor (f) in several set of models with different numbers of zoom sections (N) as Re increases, and the case where the N value is zero indicates the PTR model. In both PTR and CD-PTR, the Fanning friction factor(f) decreases with the increase of Re. And the f in CD-PTR absorber tube are always much higher than that in PTR. As the number of zoom sections (N) increases, the friction factor in CD-PTR absorber tube increases rapidly, which is caused by the obvious rise of the pressure drop caused by the introduction of the convergent-divergent structure.

Based on the analysis, when the N is increased, Nu is higher but pressure drop down is also enhanced. In order to comprehensively consider the influence of Nu and friction, the authors proposed the Thermal Efficiency Factor(TEF) to further analyze the evaluation of the thermal performance of the PTR system. The TEF is defined as follows:

Figure 19 presents the variation of the system thermal efficiency factor(TEF) with the increase of Re for CD-PTR with different number of zoom sections(N). It can be seen from the figure that the thermal efficiency factor decreases with the increase of Re, since rather than the increase of Nu, the increase of the friction factor has a more significant effect on the efficiency. It can also be seen that as the value of N increases, the thermal efficiency factor gradually decreases, which means that as the number of zoom sections increases, the impact of the sharply increased friction factor on the system efficiency is much greater than the increase of Nu. Figure 19 also shows that the thermal efficiency of CD-PTR is not always higher than that of PTR. For models with different N, within a certain Re range, the TEF of CD-PTR is higher than 1.0, which means that the overall thermal efficiency of CD-PTR is higher than that of PTR. If Re exceeds this range, the introduction of the convergent-divergent structure cannot improve the system thermal efficiency. Take the thermal efficiency factor of CD-PTR with N=10 as an example, when the Re is less than

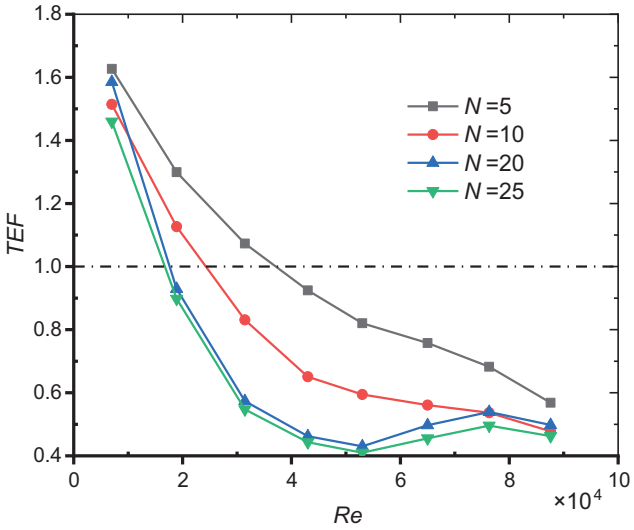

Figure 19. The variation of TEF of CD-PTR with different number of zoom sections (N).

26000, the introduction of convergent-divergent structure can enhance the overall thermal efficiency and the thermal efficiency factor reaches 1.51 when Re=7000.

CONCLUSIONS

This study proposed to apply convergent-divergent tube as PTR absorber tube (CD-PTR) for improving heat transfer performance of PTC system. The FVM method coupled with MCRT method was adopted to investigate the heat transfer performance and flow characteristics of parabolic solar collector system. The simulation results draw the conclusions.

1. With the increase of Re, the temperature distribution of cross-section become more uniform, thereby

providing better thermal conditions for absorber tube.

2. The TKE of HTF increases as the *Re* increases. At the same *Re*, the variable cross-section of the CD-PTR significantly increases local TKE, thereby accelerating the heat transfer of the coupled surface.
3. The average *Nu* of CD-PTR increases as the number of zoom sections increases, and is always higher than that of PTR. When *Re*=86400 and *N*=25, the average *Nu* increased by 66%.
4. The friction factor (*f*) gradually decreases as *Re* increases. And as the number of zoom sections increases, *f* in the CD-PTR absorber tube increases rapidly.
5. The improved CD-PTR that applied the convergent-divergent structure in PTC technology proposed in this paper has higher heat transfer efficiency than PTR within a certain range of *Re*.

NOMENCLATURE

D	Diameter of receiver, m
C_p	Heat capacity, J/(kg·K)
ρ	Density, kg/m^3
Y_M	Contribution of the fluctuating dilatation in compressible turbulence to the overall dissipation rate
G_b	Generation of turbulent kinetic energy due to buoyancy
G_k	Generation of turbulent kinetic energy due to the mean velocity gradients
S_k S_ε	User-defined source term
E_{sun}	Solar irradiance, W/m^2
P	Pressure, Pa
T	Temperature, K
v	Velocity, m/s
Re	Reynolds number
Nu	Nusselt number
q	Heat flux, W/m^2
h	Heat transfer coefficient, W/(m^2·K)
f	Fanning friction factor
Pr	Prandtl number

Greek symbols

ν	Kinematic viscosity, m^2/s
α	Absorptivity of receiver
α_v	Coefficient of expansion
Φ	Dissipation function
σ_k	Turbulent Prandtl numbers for k
σ_ε	Turbulent Prandtl numbers for ε

Subscripts

Max	Maximum temperature
Min	Minimum temperature
Exp	Experimental test
Num	Numerical simulation
s	Refers to smooth tube
f	Refers to fluid
a	Refers to environment
g	Refers to glass envelope

AUTHORSHIP CONTRIBUTIONS

Authors equally contributed to this work.

DATA AVAILABILITY STATEMENT

The authors confirm that the data that supports the findings of this study are available within the article. Raw data that support the finding of this study are available from the corresponding author, upon reasonable request.

CONFLICT OF INTEREST

The author declared no potential conflicts of interest with respect to the research, authorship, and/or publication of this article.

ETHICS

There are no ethical issues with the publication of this manuscript.

REFERENCES

[1] Hussein AK. Applications of nanotechnology in renewable energies—A comprehensive overview and understanding. Renew. Sust Energ Rev 2015;42:460−476. [CrossRef]

[2] Yan J, Chou SK, Desideri U, Tu ST, Jin HG. Research, development and innovations for sustainable future energy systems. Appl Energy 2013;112:393−395. [CrossRef]

[3] Chen X, Wang FQ, Han YF, Yu RT, Cheng ZM. Thermochemical storage analysis of the dry reforming of methane in foam solar reactor. Energy Convers Manag 2018;158:489−498. [CrossRef]

[4] Plytaria MT, Tzivanidis C, Bellos E, Energetic investigation of solar assisted heat pump underfloor heating systems with and without phase change materials. Energy Convers Manag 2018;173:626−639. [CrossRef]

[5] Liang HX, Wang FQ, Cheng ZM, Xu C, Li GQ. Full-Spectrum Solar Energy Utilization and Enhanced Solar Energy Harvesting via Photon Anti-Reflection and Scattering Performance Using Nanophotonic Structure. ES Energy Environ 2020;8:29−41.

[6] Yildırım C. Performance analysis and design of liquid based solar heating system. J Therm Eng 2018;5:1702-1712.

[7] Behar O, Khellaf A, Mohammedi K. A review of studies on central receiver solar thermal power plants. Renew Sust Energ Rev 2013;23:12−39. [CrossRef]

[8] Wang FQ, Cheng ZM, Tan JY, Yuan Y, Shuai Y, Liu LH. Progress in concentrated solar power technology with parabolic trough collector system: A comprehensive review. Renew Sust Energ Rev 2017; 79:1314−1328. [CrossRef]
[9] Hernandez RR, Easter SB, Murphy-Mariscal ML, Maestre FT, Tavassoli M, Allen EB, et al. Environmental impacts of utility-scale solar energy. Renew Sust Energ Rev 2014; 29:766−779. [CrossRef]
[10] Mao QJ, Chen HZ, Zhao YZ, Wu HJ. A novel heat transfer model of a phase change material using in solar power plant. Appl Therm Eng 2018;129:557−563. [CrossRef]
[11] Sathish Kumar Gurupatham, Govindasamy K. Manikandan, Fahad Fahad. Harnessing and storing solar thermal energy using phase change material (pcm) in a small flat plate collector. J Therm Eng 2020;6:511−520. [CrossRef]
[12] Wang FQ, Shuai Y, Tan HP, Yu CL. Thermal performance analysis of porous media receiver with concentrated solar irradiation. Int. J. Heat Mass Transf 2013;62:247−254. [CrossRef]
[13] Sarwar J, Georgakis G, Kouloulias K, Kakosimos KE. Experimental and numerical investigation of the aperture size effect on the efficient solar energy harvesting for solar thermochemical applications. Energy Convers Manag 2015;92:331−341. [CrossRef]
[14] Ahlem Bouguila, Rachid Said. Optimization of a Small Scale Concentrated Solar Power Plant Using Rankine Cycle. J Therm Eng 2020;6:268−281. [CrossRef]
[15] Bellos E, Tzivanidis C, Belessiotis .VDaily performance of parabolic trough solar collectors. Sol Energy 2017;158:663−678. [CrossRef]
[16] Khanna S, Newar S, Sharma V, Panigra hi PK, Mallick TK. Deformation of receiver in solar para-bolic trough collector due to non uniform tempera-ture and solar flux distribution and use of bimetallic absorber tube with multiple supports.. Energy 2018;165:1078−1088. [CrossRef]
[17] Wang K, He YL, Cheng ZD. A design method and numerical study for a new type parabolic trough solar collector with uniform solar flux distribution. Sci China Technol Sci 2014;57:531−540. [CrossRef]
[18] Mao QJ. Recent developments in geometrical configurations of thermal energy storage for concentrating solar power plant. Renew Sust Energ Rev 2016;59:320−327. [CrossRef]
[19] Mokhtar Ghodbane, Boussad Boumeddane, Ahmed Kadhim Hussein, Dong Li, S. Sivasankaran. Optical numerical investigation of a solar power plant of parabolic trough collectors. Journal of Thermal Engineering 2021;7: 550-569. [CrossRef]
[20] Liu P, Zheng NB, Liu ZC, Liu W. Thermal-hydraulic performance and entropy generation analysis of a parabolic trough receiver with conical strip inserts. Energy Convers Manag 2019;179:30−45. [CrossRef]
[21] Farhad Afsharpanah, Amirhossein Zabihi SheShpoli, Khashayar Pakzad, Seyed Soheil Mousavi Ajarostaghi. Numerical investigation of non-uniform heat transfer enhancement in parabolic trough solar collectors using dual modified twisted-tape inserts. J Therm Eng 2021;7:133−147. [CrossRef]
[22] Keykhah S, Assareh E, Moltames R, Taghipour A, Barati H. Thermoeconomic analysis and multi-objective optimization of an integrated solar system for hydrogen production using particle swarm optimization algorithm. J Therm Eng 2021;7: 746−760. [CrossRef]
[23] Liang HX, Wang FQ, Zhang D, Cheng ZM, Zhang CX, Lin B, et al. Experimental investigation of cost-effective ZnO nanofluid based spectral splitting CPV/T system. Energy 2020;194:116913. [CrossRef]
[24] Salem TK, Khosroshahi FS, Arik M, Hamban MO, Budakli M. Numerical and experimental analysis of a heat-pipe-embedded printed circuit board for solid state lighting applications. Exp Heat Transf 2019;32:1−13. [CrossRef]
[25] Karbasi E, Karimi-Sabet J, Mohammadi-Rovshandeh J, Moosavian M.A, Ahadi H, Amini Y. Experimental and numerical study of air-gap membrane distillation (AGMD): Novel AGMD module for Oxygen-18 stable isotope enrichment. Chem Eng J 2017;322:667−678. [CrossRef]
[26] Amini Y, Mokhtari M, Haghshenasfard M, Gerdroobary MB. Heat transfer of swirling impinging jets ejected from Nozzles with twisted tapes utilizing CFD technique. Case Stud Therm Eng 2015;6:104−115. [CrossRef]
[27] Hashemipour N, Karimi-Sabet J, Motahari K, Monfared S.M, Amini Y, Moosavian MA. Experimental and simulation investigation on separation of binary hydrocarbon mixture by thermogravitational column. J Mol Liq 2018; 268:791−806. [CrossRef]
[28] Chen ZJ, Wang DC, Feng M. Numerical Simulation on Heat Transfer Comprehensive Performance of Different Convergent-Divergent Tubes. Press Vessel Technol 2013;30:37−41.
[29] Wang FQ, Tang ZX, Gong XT, Tan JY, Han HZ, Li BX. Heat transfer performance enhancement and thermal strain restrain of tube receiver for parabolic trough solar collector by using asymmetric outward convex corrugated tube. Energy 2016;114:275−292. [CrossRef]
[30] Wang FQ, Lai QZ, Han HZ, Tan JY. Parabolic trough receiver with corrugated tube for improving heat transfer and thermal deformation characteristics. Appl Energy 2016;164:411−424. [CrossRef]
[31] Zhang YJ, Ouyang R, Deng XH, Li ZW. Natural convection boiling heat transfer in enhanced heat

transfer tubes. J South China Uni Technol (Natural Science Edition) 2004 ;32:41−43.
[32] Jin ZL, Dong QW, Liu MS, Zhang FQ. Numerical research on optimization of the convergent-divergent tube structure. Journal of Zhengzhou University (Engineering Science) 2010;31:105−107.
[33] Pandey M, Padhi BN, Mishra I. Numerical simulation of solar parabolic trough collector with arc-plug insertion. Energy Sources A Recovery Util Environ Eff 2020;43:2635−2655. [CrossRef]
[34] Li D, Li Z, Zheng Y, Liu C, Hussein AK, Liu, X. Thermal performance of a PCM-filled double-glazing unit with different thermophysical parameters of PCM. Sol Energy 2016;133:207−220. [CrossRef]
[35] Liu C, Wu Y, Li D, Ma T, Hussein AK, Zhou Y. Investigation of thermal and optical performance of a phase change material–filled double-glazing unit. J Build Phys 2018; 42:99−119. [CrossRef]
[36] Amini Y, Esfahany MN. CFD simulation of the structured packings: A review. Separation science and technology 2019;54:2536−2554. [CrossRef]
[37] Zheng S, Yang Y, Sui R, Lu Q. Effects of C2H2 and C2H4 radiation on soot formation in ethylene/air diffusion flames. Appl Therm Eng 2021;183:116194. [CrossRef]
[38] Sheikholeslami M. New computational approach for exergy and entropy analysis of nanofluid under the impact of Lorentz force through a porous media. Comput Methods Appl Mech Eng 2019;344:319−333. [CrossRef]
[39] Hussein AK, Walunj A, Kolsi L. Applications of nanotechnology to enhance the performance of the direct absorption solar collectors. J Therm Eng 2016; 2:529−540. [CrossRef]
[40] Hussein AK, Li D, Kolsi L, Kata S, Sahoo B. A review of nano fluid role to improve the performance of the heat pipe solar collectors. Energy Procedia, 2017;109:417−424. [CrossRef]
[41] Hussein AK. Applications of nanotechnology to improve the performance of solar collectors – Recent advances and overview. Renew Sust Energ Rev 2016; 62:767−792. [CrossRef]
[42] Khanna S, Singh S, Kedare SB. Explicit expressions for temperature distribution and deflection in absorber tube of solar parabolic trough concentrator. Solar Energy 2015;114:289−302. [CrossRef]
[43] Jebasingh VK, Herbert GMJ. A review of solar parabolic trough collector. Renew Sust Energ Rev 2016;54:1085−1091. [CrossRef]
[44] Khanna S, Kedare SB, Singh S. Deflection and stresses in absorber tube of solar parabolic trough due to circumferential and axial flux variations on absorber tube supported at multiple points. Solar Energy 2014;99:134−151. [CrossRef]
[45] Wang XZ, He YR, Cheng G, Shi L, Liu X, Zhu JQ. Direct vapor generation through localized solar heating via carbon-nanotube nanofluid. Energy Convers Manag 2016;130:176−183. [CrossRef]
[46] Ahmed MH. Two dimension numerical modeling of receiver tube performance for concentrated solar power plant. Energy Procedia 2014;57:551−560. [CrossRef]
[47] Yilmaz IH, Söylemez MS. Thermo-mathematical modeling of parabolic trough collector. Energy Convers Manag 2014;88:768−784. [CrossRef]
[48] Mwesigye A, Bello-Ochende T, Meyer JP. Heat transfer and thermodynamic performance of a parabolic trough receiver with centrally placed perforated plate inserts. Appl Energy 2014;136:989−1003. [CrossRef]
[49] Wang FQ, Tan JY, Ma LX. Effects of glass cover on heat flux distribution for tube receiver with parabolic trough collector system. Energy Convers Manag 2015;90:47−52. [CrossRef]
[50] Manikandan GK, Iniyan S, Goic R. Enhancing the optical and thermal efficiency of a parabolic trough collector – A review. Appl Energy 2019; 235:1524−1540. [CrossRef]
[51] Gong XT, Wang FQ, Wang HY, Tan JY, Lai QZ, Han HZ. Heat transfer enhancement analysis of tube receiver for parabolic trough solar collector with pin fin arrays inserting. Sol Energy 2017;144:185−202. [CrossRef]
[52] Islam M, Saha SC, Yarlagadda PKDV, Karim A. A tool to minimize the need of Monte Carlo ray tracing code for 3D finite volume modelling of a standard parabolic trough collector receiver under a realistic solar flux profile. Energy Sci Eng 2020;8:3087−3102. [CrossRef]
[53] Qiu Y, Li MJ, Wang K, Liu ZB, Xue XD. Aiming strategy optimization for uniform flux distribution in the receiver of a linear Fresnel solar reflector using a multi-objective genetic algorithm. Appl Energy 2017;205:1394−1407. [CrossRef]
[54] Wu ZY, Lei DQ, Yuan GF, Shao JJ, Zhang YT, Wang ZF. Structural reliability analysis of parabolic trough receivers. Appl Energy 2014;123:232−241. [CrossRef]
[55] Roldán MI, Valenzuela L, Zarza E. Thermal analysis of solar receiver pipes with superheated steam. Appl Energy 2013;103:73−84. [CrossRef]
[56] Launder BE, Spalding DB. Lectures in Mathematical Models of Turbulence., London, England: Academic Press; 1975.
[57] Wu ZY, Li SD, Yuan GF, Lei DQ, Wang ZF. Three-dimensional numerical study of heat transfer characteristics of parabolic trough receiver. Appl Energy 2014;113:902−911. [CrossRef]